Report no. changed (Mar 2006): SM-223-UU

SACLANTCEN MEMORANDUM
serial no.: SM-223

SACLANT UNDERSEA RESEARCH CENTRE

MEMORANDUM

# Transmission-time variability, vertical spatial and temporal analysis of NAPOLI '85, an experiment in the Tyrrhenian Sea

J.R. Potter, T. Akal
and B.J. Uscinski

September 1989

Page count for SM-223
(excluding covers)

| Pages | Total |
|---|---|
| i–vi | 6 |
| 1–31 | 31 |
| | 37 |

SACLANT Undersea Research Centre
Viale San Bartolomeo 400
19026 San Bartolomeo (SP), Italy

tel: 0187 540 111
telex: 271148 SACENT I

NORTH ATLANTIC TREATY ORGANIZATION

Report no. changed (Mar 2006): SM-223-UU



# Transmission-time variability, vertical spatial and temporal analysis of NAPOLI '85, an experiment in the Tyrrhenian Sea

J.R. Potter, T. Akal
and B.J. Uscinski

The content of this document pertains to work performed under Project 05 of the SACLANTCEN Programme of Work. The document has been approved for release by The Director, SACLANTCEN.

Issued by:
Underwater Research Division

J.M. Hovem
J.M. Hovem
Division Chief

Report no. changed (Mar 2006): SM-223-UU





intentionally blank page

# Transmission-time variability, vertical spatial and temporal analysis of NAPOLI '85, an experiment in the Tyrrhenian Sea

J.R. Potter, T. Akal and B.J. Uscinski

**Executive Summary:** The performance of sonar systems is affected by sound-speed variability in the ocean, which frequently takes the form of patches of water with relatively high or low sound-speed. These patches sometimes focus the sound and at other times de-focus the sound, depending on the positions of source and receiver with respect to the patches, which may be randomly distributed. This focusing and de-focusing results in submarine detection where it would not normally be obtained and loss of target respectively. A unified approach or a theory which explains all the physics of the phenomena does not yet exist.

NAPOLI '85 was a propagation experiment which recorded signals from small explosive charges at two vertical arrays. The experiment was designed so that sound propagating along two paths, one of which runs deep and the other passes near the surface, neither interact with the surface or bottom could be separated. This allows us to compare the results with an existing theory which describes one aspect of sound propagation variability. By comparing the signal received at the two arrays, the variability in amplitude and arrival-time of the signals imposed by the ocean over each acoustic path, as a function of frequency from 250 to 2000 Hz, could be determined. This acoustic variability changed both with depth and with time, during the 3 days of the experiment.

This memorandum describes the experiment and analyses the arrival-time variability for acoustic energy propagating. Sound-speed data, collected by a towed instrument with high horizontal and vertical resolution, were used to obtain a picture of the medium between the arrays for input to theory. The arrival-time variability is presented as a function of depth down the array and time for each of the two paths. The near-surface path accrues 3 times as much variability in arrival-time (0.3 ms) as the deeper path. The vertical spatial structure of the variability is shown to be correctly predicted by theory.

Further work is in progress to analyse the acoustic intensity variations and to prepare a memorandum on the environmental data analysis.

intentionally blank page

# Transmission-time variability, vertical spatial and temporal analysis of NAPOLI '85, an experiment in the Tyrrhenian Sea

J.R. Potter, T. Akal and B.J. Uscinski

**Abstract:** An acoustic propagation experiment (NAPOLI '85) was carried out in the Tyrrhenian Sea in October 1985 in which signals from a broadband source were recorded at a range of 5 km with a vertical 62-m hydrophone array over a period of five days. The experiment was designed to investigate the transfer function of the ocean medium over an acoustic frequency range from 250 Hz to 2 kHz as a function of time and position down the vertical array. This memorandum describes the experiment and treats the pulse arrival times for one ray path, the lower refracted path. In contrast to most previous experiments of this type, the sound-speed refractive index variability was dominated by non-internal-wave features. Some of the implications of this (regarding input to the scattering theory and acquiring environmental measurements) are explored. The experimental spatial structure function of the arrival time down the vertical array is presented and shown to compare well, given the limitations of the data, with theoretical predictions both as regards its magnitude and functional behaviour.

**Keywords:** acoustic ○ broadband ○ fluctuations ○ internal wave ○ Mediterranean ○ model ○ profiles ○ random ○ scattering ○ sound-speed ○ stochastic ○ transmission-time ○ Tyrrhenian ○ variability

## Contents



**Acknowledgement:** The authors wish to thank the many support group personnel at SACLANTCEN whose efforts and enthusiasm made the experiment a success. We are indebted to the Italian Navy for the use of their research vessel *Magnaghi*. The authors owe particular recognition to Dr. R. Thiele, whose comments identified several misconceptions and had a profound influence on the final memorandum. Final thanks go to A. Trangeled, whose 'delicious' software has greatly assisted with the data analysis and graphics.

# 1
# Introduction

For many years there has been considerable interest in the random fluctuations that arise in a sound field propagating in the ocean. These fluctuations are produced by scattering from irregular structures that affect the acoustic refractive index. Several major experiments have been carried out in order to investigate these fluctuations, including those made at Cobb Seamount [1,2] in 1971 and 1977, and in the Azores [3]. Until now the majority of experiments have measured the acoustic fluctuations with one, or possibly two, receivers over several days at a time. Thus they have provided data that give a good description of the fluctuations in time but give little information as to their spatial structure. NAPOLI '85 was designed to measure the spatial characteristics of the acoustic field in the vertical direction and their variation with time.

This memorandum describes the design and conduct of the experiment. It also gives an analysis of the relative arrival times of the lower refracted path (hereafter referred to as the 'direct' path) as received down a vertical array. The use of a broadband source is an important feature of NAPOLI '85 since a range of temporal acoustic frequencies is thus transmitted and received simultaneously. The resulting data will hopefully allow the ocean transfer function (the acoustic response of the ocean when the input signal is an impulse) to be reconstructed for all frequencies in a 2-kHz bandwidth. Another important aspect of the broadband feature is that it allows the cross-correlation of intensity fluctuations at different frequencies to be obtained experimentally. Different acoustic frequencies produce different patterns of intensity fluctuation when propagating through a random medium. Theoretical work of the cross-correlation of such patterns suffers from certain significant limitations [4,5], and the availability of experimental cross-correlations over a continuous frequency range could well prove useful in resolving some of these difficulties. The equivalent results from other experiments cover at most only four discrete frequencies [2,6].

A similar acoustic propagation experiment, the AIWEX Acoustic Transmission Experiment (AATE), was conducted under the Arctic ice in March 1985; the data are still in the process of being analysed (T.E. Ewart, personal communication). The sound-velocity profile and range of propagation were similar to those of NAPOLI '85. In AATE the sound-field profile was measured continuously in space and time (at a fixed source-receiver distance) at four discrete acoustic frequencies of 2, 4, 8 and 16 kHz. The AATE and NAPOLI '85 are thus complementary.

Most of the acoustic fluctuation experiments that have been carried out have used either towers set on the sea floor or sub-surface arrays anchored directly to the bottom. NAPOLI '85 used an array which was supported by surface-deployed flotation, indirectly anchored to the bottom. For phase fluctuations, this method is not a good one. We were fortunate that exceptionally good weather prevailed during the experiment reducing array motion to a level where relative arrival times could be analysed. The method is certainly a good one for the analysis of intensity fluctuations, and applicable to the open ocean since a stable platform, such as the Arctic ice sheet, is not needed in order to suspend the array.

This project was undertaken as a joint venture by the SACLANT Undersea Research Centre, La Spezia, Italy and the Ocean Acoustics Group, DAMTP, Cambridge University, UK.

# 2

# Description of the experiment

## 2.1. AREA

The Tyrrhenian Sea is one of the major basins of the Mediterranean Sea and is connected to the western Mediterranean via the large Sardinia–Sicily Channel. There are also small connections through the Messina and Bonifacio Straits and Corsica Channel. The basin forms part of the western Mediterranean, where SACLANTCEN has conducted extensive oceanographic studies (e.g. Molcard and Tait [7], Hopkins and Zanasca [8]).

In order to avoid an overlapping multiple acoustic arrival structure with bottom reflections, the experimental site was selected in the central Tyrrhenian Sea where the water depth is 3600 m (Fig. 1). During the whole experimental period, wind and sea conditions were extremely calm. Sea-state was zero most of the time with no wind.

## 2.2. EXPERIMENTAL CONFIGURATION

Some equipment limitations on signal bandwidth and data-link receiving range had to be balanced against the ideal frequency and transmission range in order to arrive at a realistic experimental design in which the sound would be multiply scattered and exhibit fluctuations in intensity and phase. The resulting experimental configuration is shown schematically in Fig. 2. The research vessel *Maria Paolina G.* (MPG) both deployed small electrically detonated explosive charges (2.75 g TNT) at a depth of 400 m and acquired data from two hydrophone arrays anchored some 5 km apart. The first array of four hydrophones (at depths of 10, 85, 160 and 308 m) was deployed close to the MPG as a reference array to obtain the undistorted signature of each signal. The second array, some 5 km distant from the first, was a vertical array consisting of 32 hydrophones with a regular 2-m spacing which recorded the scattered signals. To ensure that the signals were all generated at the same depth, the sources were lowered on a wire of fixed length and detonated electrically. Signals received by the arrays were low-pass-filtered and transmitted back to the ship via a radio link in digital format within a frequency band from 10 Hz to 3 kHz.

The strength of fluctuations in the acoustic refractive index tends to decrease with depth, so that rays travelling near the surface undergo more scattering and provide more interesting data than rays which travel at greater depths. The upper hy-

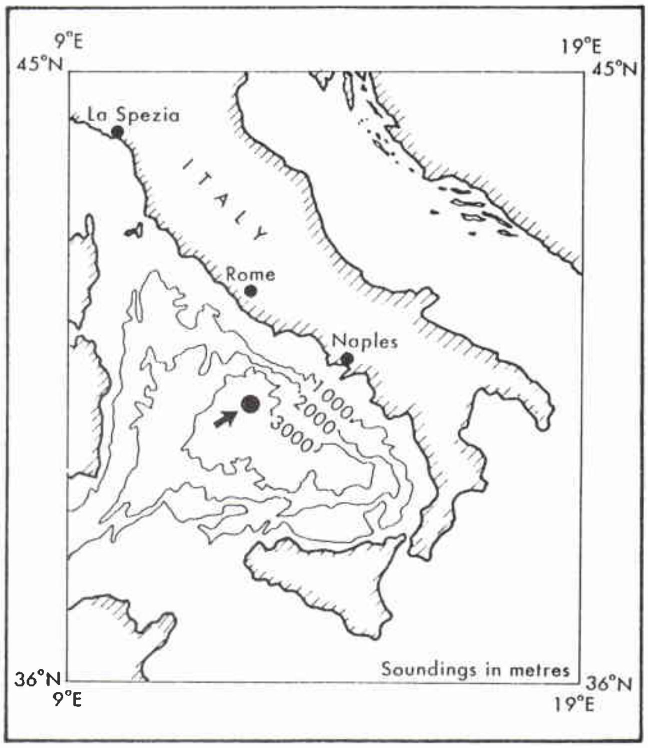


*Fig. 1.* Map of the NAPOLI '85 experimental area. The acoustic arrays were moored at the point indicated by the arrow.

drophone of the vertical array was therefore positioned at 224 m, as near the surface as possible consistent with maintaining a separation between the lower-refracted ray and surface-reflected/refracted rays. The depths of the top and bottom of the vertical array were monitored by pressure sensors at each end of the array. The source and receiver depths had to be arranged so that multipath arrivals would occur at well-separated times at the vertical array. This requirement forced us to detonate the sources at 400 m, below the region of most sound-speed inhomogeneities and the operating depth range of the towed oscillating body (TOB) which provided conductivity, temperature and pressure data.

Theoretical calculations yield the correlation time of sound fluctuations induced by inhomogeneities with spatial scales relevant to the source frequencies and transmission range. Accordingly, NAPOLI '85 was conducted over a period of five days with a time interval between detonations of 60 min for days 1 and 5, 30 min for days 3 and 4, and 15 min for day 2.

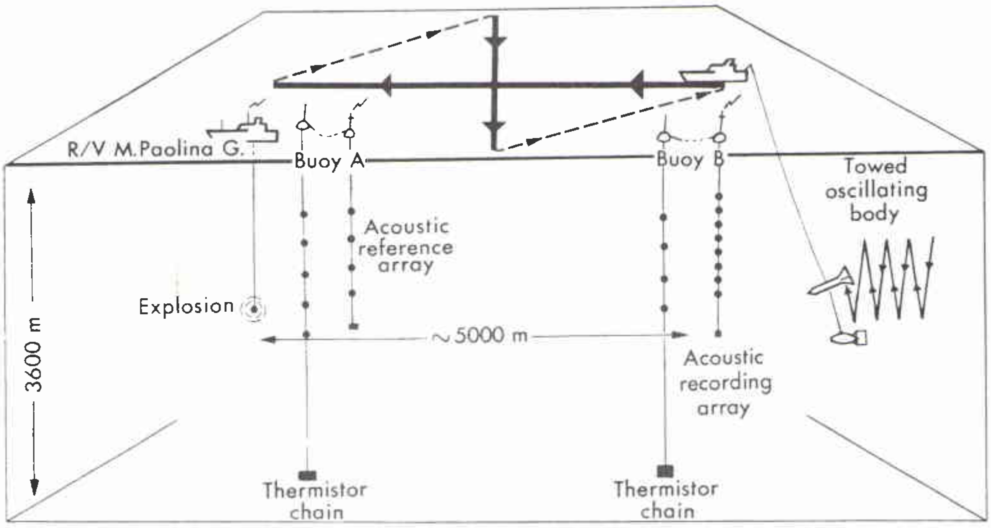


*Fig. 2.* Illustration of the acoustic and environmental measurement systems. The *Maria Paolina G.* (MPG) deployed the sources and acquired acoustic data. The research vessel *Magnaghi* towed the TOB with CTD sensors in a cruciform path, shown as a solid line. The moorings for both the reference array (buoy A) and the 32-hydrophone vertical array (buoy B) incorporated thermistor chains.

The MPG, and hence the sources, were kept as far as possible in line with the two arrays. During the 5-day period, the maximum deviation from linearity was $10^\circ$. The distance from the MPG to the first reference array was $0.56 \pm 0.24$ km throughout the experiment.

### 2.3. *ACOUSTIC MEASUREMENTS*

The data acquisition and reduction processes are divided into three distinct parts: the vertical array and associated electronics, the ship's acquisition system, and the subsequent analysis at SACLANTCEN.

*Vertical array* Of the 32 hydrophones, 6 were found to be unreliable. Each of the remaining 26 hydrophones had a pre-amplifier and low-pass filter. The low-pass filter attenuated by 3 dB at 2 kHz and 90 dB at 3 kHz. An electronics package at the head of the hydrophone string sampled the filtered output from the hydrophones at 6 kHz sampling rate. The data were digitised and multiplexed before transmission by radio to the receiving ship.

*Receiving ship* The receiving system on board the MPG consisted of a radio link with the hydrophone array buoys and a digital recording medium to record the data exactly as it was received.

*Data analysis* The recorded data was played back and de-multiplexed to give 26 reliable channels of data. Since the data had been low-pass-filtered with a pass band below 2 kHz before sampling at 6 kHz, the values of the original filtered data before sampling can be recovered within the digital resolution of 72 dB. In practice, the signal-to-noise ratio (SNR) limits the identification of the time at which the signal arrives. For our case (SNR $\simeq$ 40 dB) the maximum realistic time resolution for the purpose of identifying the signal arrival time is $\sim 8\mu$s (see Subsect. 2.5).

Since the broadband signal undergoes distortion during transmission through the (mildly dispersive) medium there is no unique definition of arrival time. We began by defining the arrival time as the position of the first peak in the received signal. Later, we changed this definition to be the lag at which the maximum output was obtained from a replica-correlator. It was found that all the pulses received by the lower refracted path were very similar. A replica was created by taking a representative received signal from one of the events. This latter definition should provide a slightly more robust estimate of the arrival time which takes into account frequencies in the signal from 250 Hz to 2 kHz. Comparison with the results obtained from the earlier definition showed very little difference between the two methods.

A possible difficulty arises if there is differential horizontal motion of the hydrophones in the vertical array. The time resolution obtained from the interpolating filter is equivalent to a horizontal motion of a receiver of only 12 mm. If the horizontal motion of individual hydrophones with respect to other hydrophones in the vertical array is more than this, array motion will contaminate the relative arrival-time data.

Calculations were made to assess the dynamic stability of the array elements using a model of the array response to a known current profile. No current measurements were taken during NAPOLI '85 so values had to be estimated, making the calculation speculative. Using a mean current speed of 0.05 ms$^{-1}$ with a variability of some $\pm 25\%$ over a time-scale relevant to the fluctuations (several hours) the calculated horizontal rms fluctuation in relative hydrophone displacement is 60 mm. This value is equivalent to five times the time resolution of the interpolated data and represents a serious possible cause for concern.

To test this possible source of error, the relative arrival times were calculated for both the direct path and the surface-refracted path. If array motion were contaminating the data, the effect would be present in the relative arrival times of both paths. If the relative arrival times are determined only by the inhomogeneities encountered (and hence by the path history) then the two paths should be uncorrelated. The situation is statistically complicated by the higher fluctuation values of the upper path, which tend to mask possible correlations with the lower path. By examining subsets of the total ensemble of events the following statistically significant result is obtained. At the 60% confidence level, the contribution of array motion to the total variance of relative arrival times of the lower path is less than 20%, with an expected value indistinguishable from zero. We therefore propose that array motion has not significantly contaminated the data.

### *2.4. ENVIRONMENTAL MEASUREMENTS*

Whilst the MPG collected the acoustic data, a second ship, the Italian Navy research vessel *Magnaghi*, operated the TOB. The depth of the TOB was made to oscillate between 25 and 250 m. Deeper oscillations were not possible due to constraints on the minimum steerage speed of the *Magnaghi*. The TOB was towed along a path parallel to the acoustic propagation path and then perpendicular to it (Fig. 2). The TOB was towed along at 0.75–1.5 $\mathrm{ms}^{-1}$ with each 'leg' of the 'zig-zag' path at $\sim 45°$ to the vertical. Both the vertical and horizontal speeds of the TOB sensors are thus $\sim$ 0.5–1.0 $\mathrm{ms}^{-1}$. The data were sampled at 12 Hz, providing a vertical resolution of better than 0.1 m. The data were filtered to reduce noise with a concomitant degradation of vertical resolution to 1 m. A total of 14 TOB casts were made, of various durations from 20 min to 5 h. Figure 3 displays some of the TOB data and a plot of the mean sound-speed profile with successive TOB 'zigs' and 'zags' shown offset for clarity. Successive TOB 'profiles' are taken some 300 m apart horizontally and some 6 min apart in time.

A data reduction procedure was employed to expunge erroneous values and then to filter and average the TOB data, which provided a very stable and reliable set of values for each vertical metre. Ship navigational information was incorporated to provide a mapping of the TOB data into real space. The sound speed at each point was calculated from pressure, conductivity and temperature and the sound-speed field was obtained by interactively-controlled interpolation between data points. The potential density, salinity and potential temperature fields were obtained in the same way.

For frequencies of 250–2000 Hz, the range of acoustic wavelengths of interest is $\sim$ 0.75–6.0 m. Oceanic variability on the scale of a few metres or larger will therefore be 'seen' by the propagating acoustic field. The ocean medium is strongly horizontally stratified, with horizontal/vertical length scale factors of between 50 : 1 and 250 : 1. The vertical length scale of ocean inhomogeneities of interest to us therefore extends upwards of a few metres, and the horizontal from some 500 m. The vertical resolution of the TOB data is therefore sufficient, and the horizontal resolution barely so. The time period over which the TOB samples one inhomogeneity is short enough compared with the expected lifetime of these features to neglect non-synoptic contamination of the spatial data. A complete TOB cast represents data acquired over a period of some 4 h. These data enable us to establish the sound-speed field as a function of space. This allows us to calculate the mean sound-speed profile, used in the ray theory calculations, and the vertical and horizontal autocorrelation

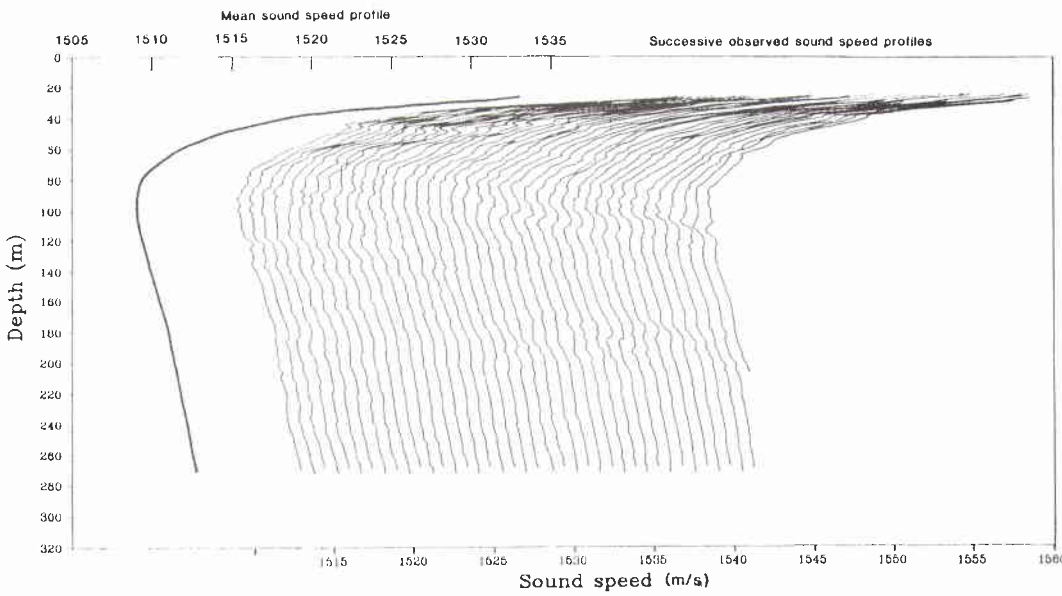


*Fig. 3.* Consecutive sound-velocity profiles, each offset by 0.75 $ms^{-1}$ from the previous profile, for a sample TOB track. The scale relevant to the first profile is written at the bottom of the figure. Fluctuations in the sound-speed profiles are clearly seen to be correlated from one profile to the next and to evolve with increasing range and time. The mean profile over all TOB data is shown as a thick solid line at the far left of the figure with the scale written above.

function (acf) of the inhomogeneities in the sound-speed field. The two-dimensional acf is important for calculating parameters used in the scattering theory to predict the structure function of the relative arrival times.

Moored thermistor chains were also deployed at the two array sites (Fig. 2), but showed temperature variations only slightly greater than the instrumental resolution. Of greater use were 4 CTD and some 70 XBT casts made from the MPG during the experiment.

### *2.5. ASSESSMENT OF ARRIVAL-TIME ACCURACY*

It was not clear to what time resolution the 6 kHz data could be meaningfully interpolated for the purpose of calculating the arrival time (defined as the time of the first peak in the signal). Interpolation was performed using a 200-point digital linear interpolating filter, which had the same frequency characteristics as the low-pass filter applied to the data prior to sampling. By applying this filter the full signal, after filtering but before sampling, was reconstructed with a sampling frequency of

120 kHz. There are three practical limitations to this procedure for assessing the arrival time of the pulse:

(i) The digital conversion of the sampling has a finite resolution.

(ii) The interpolating filter has deficiencies in its performance.

(iii) The signal is contaminated by noise which limits the identification of the arrival time, even given a perfect reconstruction of the filtered signal.

The resolution of the digital conversion is 72 dB. This is much higher than the SNR encountered, which was some 40 dB. Point (i) is therefore not significant relative to point (iii).

To test the interpolating filter, a program was developed which constructed synthetic signals from the addition of sine functions with amplitudes set to measured values from the data at $^1/_3$-octave frequency bands. The phases were nominally phase-locked, with some randomising component to represent dispersion etc. over the transmission path. The amount of phase randomisation was interactively controlled. The synthetic signals were defined at a sampling frequency of 480 kHz. Numerous runs of this numerical testing program were made and determined that, in the absence of noise, the interpolator had an rms error of 4 $\mu$s in the estimation of the signal peak.

To estimate the effect of noise contamination, it is fairly straightforward to perform an analytic calculation given the assumption of gaussian noise. Inspection of the signal form shows that the first peak can be well approximated by a sine wave of some 500 Hz frequency. For a given SNR, the probability that noise will locally misplace the peak can be written down as a function of time displacement. For an SNR of 40 dB, the 50% confidence limit for the identification of the signal peak was found to occur at a time displacement of 12 $\mu$s. This is by far the largest error component in the identification of the signal peak and is therefore the limiting factor.

The interpolating filter provided values at 120 kHz sampling frequency, providing 8 $\mu$s time resolution. We conclude that this interpolation filter provides the maximum useful time resolution. The use of a replica-correlator to define the arrival-time instead of the first peak in the signal has no significant effect on the arrival-time results.

# 3

# Discussion of direct-path arrival-time results

The principal types of eigenrays from the source to the hydrophones at each end of the vertical array are shown in Fig. 4. These rays were calculated using ray theory with a sound-velocity profile taken to be the mean measured profile. The eigenrays shown are the direct ray, an upper-refracted ray and an upper-reflected ray. At each hydrophone, the pulses which arrive by the various eigenpaths are received at times which vary with the position of the hydrophone in the array. This is a deterministic effect. There will also be small random delays caused by stochastic irregularities in the acoustic refractive index. It is these stochastic delays which we wish to investigate.

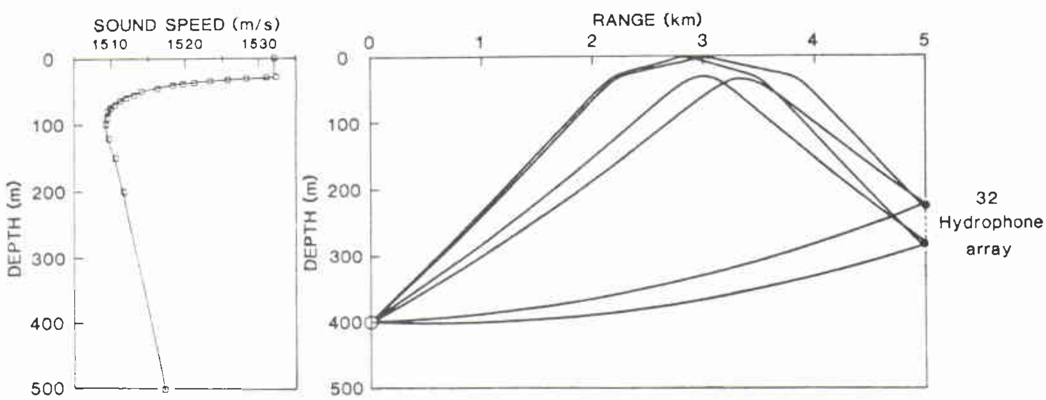


*Fig. 4.* Principal eigenrays (calculated from ray theory) connecting the source with the top and bottom of the 32-hydrophone vertical array. The sound-speed profile used in the ray-tracing model is shown on the left, with rectangles denoting the data points used for the ray-tracing.

An example from the data shows the principal signals for all hydrophones (Fig. 5), from which the deterministic trend in arrival times along the array can be seen. Bottom-reflected signals arrive much later and have been gated out. The relative arrival times predicted for the direct ray are shown in the same figure. The predicted arrival times for the refracted and reflected rays are not shown as they are critically dependent on the exact sound-speed profile near the surface, which is highly variable.

Upper-refracted and upper-reflected rays can be seen to arrive some 20–30 ms after the direct path. The geometry of the experiment ensured that the direct path was always well separated from other arrivals.

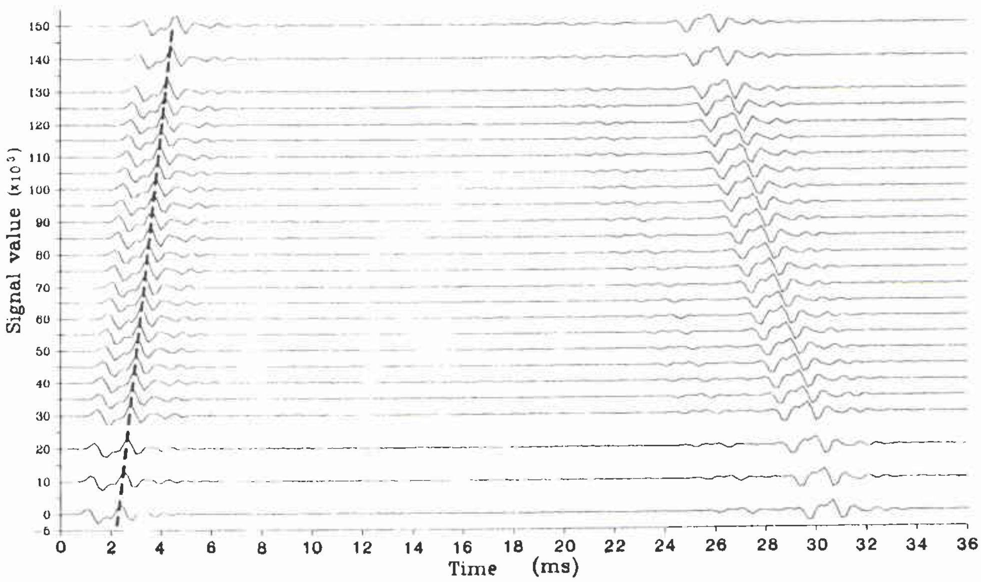


*Fig. 5.* A typical event showing the principal arrivals at all working hydrophones of the 32-hydrophone vertical array, successively offset by 2500 units on the signal value axis. The arrival time calculated from ray theory for the direct path is shown as a dashed line. Of the 32 hydrophones, numbers 1, 3, 5, 7, 29 and 31 were not operational.

### 3.1. OBSERVED RELATIVE ARRIVAL TIMES

For the following analysis we shall consider the acoustic source as situated at the origin of a cartesian set of axes ($x$, $y$, $z$, $t$), where $x$ and $z$ form the plane containing the source and receiver; $z$ is directed downwards, and $t$ is time. An illustration of the coordinate system employed is shown in Fig. 6. The arrival time at the end of the array $T(X, z')$ has been subtracted from the arrival times for all the other hydrophones to give

$$\tau(X, z) = T(X, z) - T(X, z'). \tag{1}$$

The relative arrival times have a deterministic component, which can be predicted from ray theory, and a stochastic component. The random fluctuations are masked by the (much larger) deterministic component.

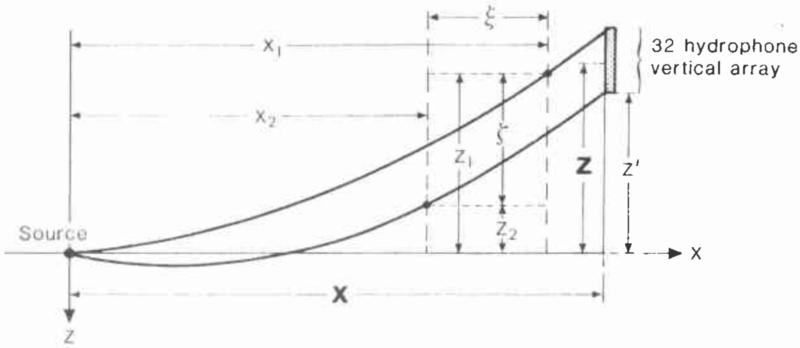


*Fig. 6.* The coordinate system used in the theoretical analysis.

### 3.2. THE DETERMINISTIC COMPONENT

The subscript $i$ will be used to denote the arrival time due to the $i$th event, i.e. detonation. The arrival-time curve is defined as the set of values $\tau_i(X, z)$ as a function of $z$. All the events have similar relative arrival-time curves, which confirms the assumption of a stable systematic lag due to the deterministic part of the sound-velocity profile. In statistical terms each event is one member of the statistical ensemble of events ($N = 229$) comprising the whole experiment. Thus, averaging over events amounts to taking an ensemble average. The mean experimental relative arrival-time curve along the array was obtained by averaging the relative arrival time at each hydrophone in the vertical array over all $N$ events:

$$\langle \tau(X, z) \rangle = (1/N) \sum_{i=1}^{N} \tau_i(X, z), \tag{2}$$

where the symbols $\langle \ldots \rangle$ denote taking the ensemble average. Provided that the $N$ events were taken over a time span much larger than the correlation period of the stochastic component, the mean arrival-time curve should approximate the deterministic arrival-time curve predicted from ray theory. To test this hypothesis, the average quantity in (2) was also formed for subsets of 25 consecutive events. These subset averages showed little variation from one to the next, confirming that the experiment did indeed span many stochastic correlation-time periods and that the deterministic component was stable. A ray-theory prediction was calculated assuming a linear profile, resulting in the rays forming arcs of circles. This (apparently over-simple) approach yielded more consistent results than a ray-tracing package (Generic Sonar Model) at SACLANTCEN. The difference between the mean deterministic delay in relative arrival times $\langle \tau(X, z) \rangle$ and the linear-profile ray-theory prediction is shown in Fig. 7. This difference (between observation and theory) is seen to be of the order of the temporal interpolation resolution. The agreement between observation and prediction is therefore very good.

More careful examination of Fig. 7 shows a systematic trend along the array, with maximum values near the upper part of the array. This trend with depth may be a result of non-linearity in the sound-speed profile, or a result of water currents displacing the array from the vertical. In the latter case, the implied horizontal array displacement is only some 0.05 m. This reinforces our belief that the currents were low and that array motion (rather than absolute displacement) is very slight and unlikely to have seriously contaminated our arrival-time data.

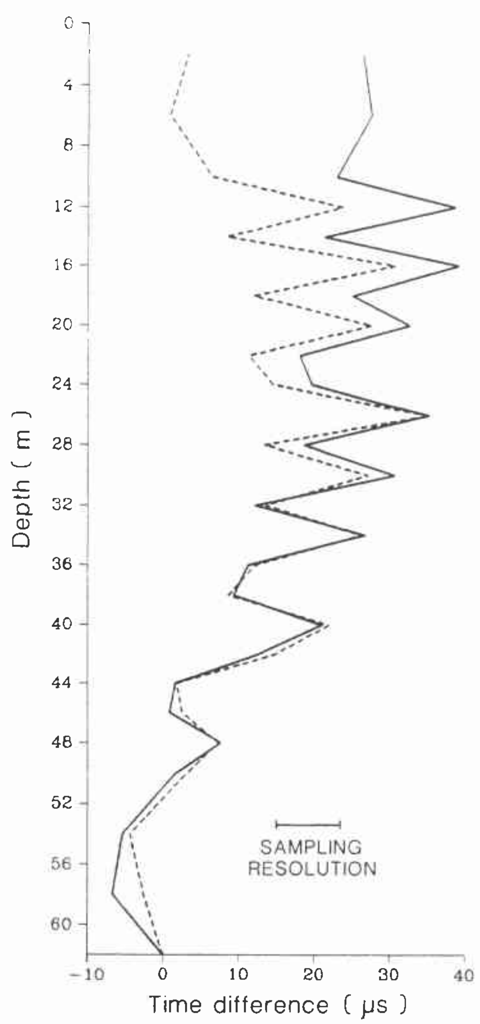


*Fig. 7.* The difference between the predicted relative arrival time calculated from ray theory and the mean arrival-time curve for all 229 events. The solid line was calculated using a range of 4.5 km and the dotted line using a range of 5.5 km. The depth (in m) is measured from the top of the recording array. The interpolated time resolution interval is shown for comparison.

### 3.3. THE STOCHASTIC COMPONENT

Subtraction of the mean delay $\langle\tau(X,z)\rangle$ from the relative arrival times gives sets of relative residual times for each event,

$$r_i(X,z) = \tau_i(X,z) - \langle\tau(X,z)\rangle, \tag{3}$$

that vary in a stochastic but correlated manner along the array and from event to event. Since the times are all relative to the lower end of the array, the residual times are constrained to be zero there. The variation in the residual arrival times at the other end of the array, however, indicates a stochastic influence. These random variations are assumed to be due to the presence of irregular sound-speed features in the ocean. The stochastic fluctuations in relative arrival times of the direct path for the whole experiment are presented as a series of contour diagrams in Fig. 8a. The corresponding fluctuations for the upper-refracted path are presented in Fig. 8b for comparison. Both Figs. 8a and b display data that have been low-pass time-filtered to remove scales of less than 1 h for ease of comparison between parts of the experiment with different sampling rates.

The first thing to note in Figs. 8a and b is that the relative arrival-time fluctuations are significantly larger than the expected errors and time resolution of the experiment. Secondly, it is clear that the upper-refracted path has an rms fluctuation some three times bigger than that of the direct path. The vertical spatial and temporal scales are, however, similar. In both cases, the vertical spatial time-delay is strongly correlated over the entire length of the vertical array, indicating that the characteristic vertical scale is larger than the array length. The temporal scale appears to be less than 4 h.

Figures 9a and b display the relative stochastic arrival-time data, without time filtering, for that period of the experiment where the sampling rate was higher than one shot each hour. Figures 9a and b show that there is considerable structure at periods of less than 1 h. Many fluctuation events appear to be very localised in time, perhaps lasting less than 30 min, separated by longer periods, of perhaps an hour or more, of relative calm. This 'bunching' of fluctuations is a characteristic feature of multiple scattering (see, for example, the MATE intensity results [2]).

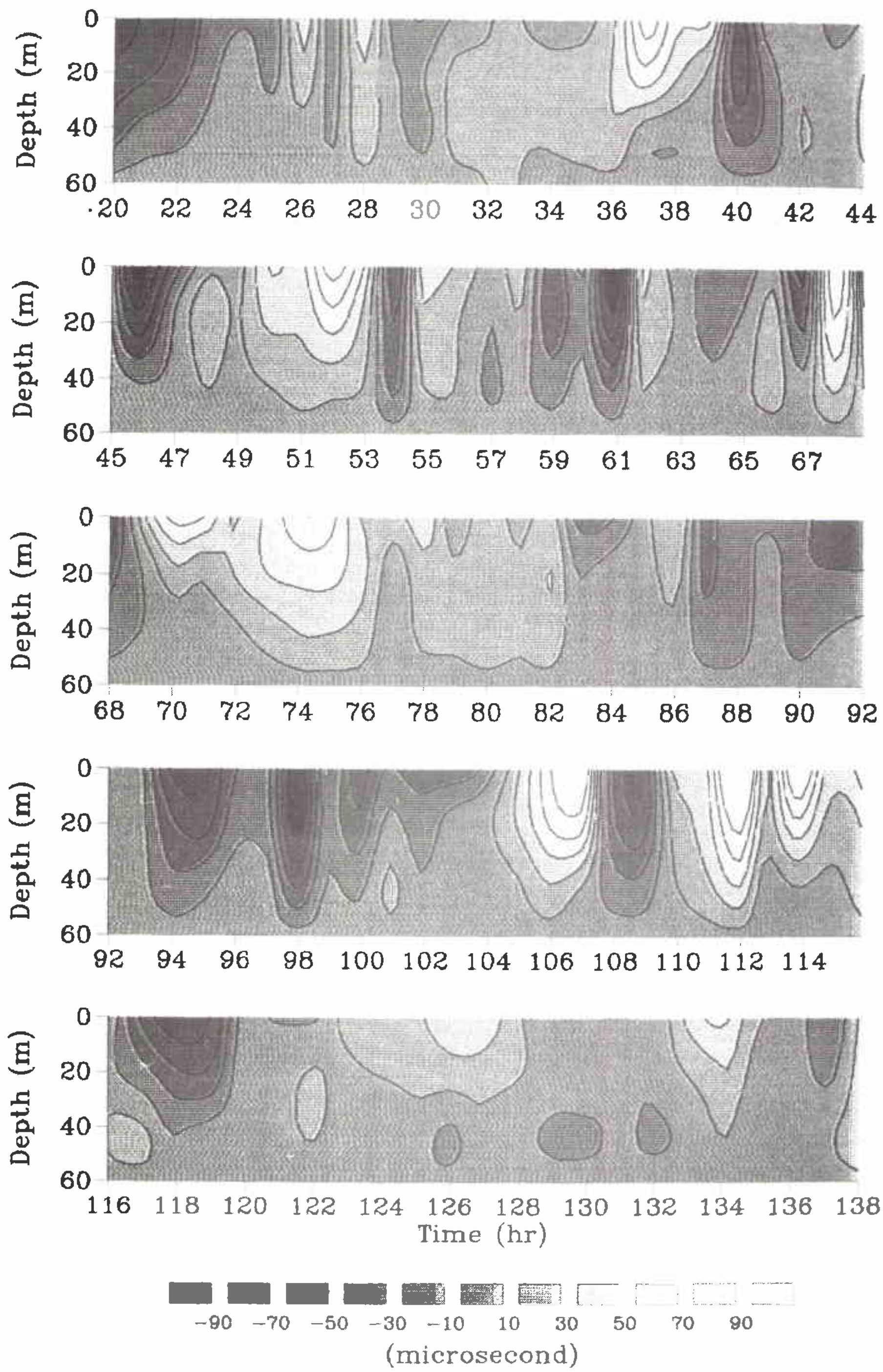


*Fig. 8a.* Contour plots of the relative stochastic arrival times for the direct ray path, for all 229 events. The time axis is the real time in hours from 00.00 h on the first day of the experiment. The vertical axis shows the depth (in m) of the receiver from the top of the array. The data have been low-pass time-filtered to facilitate comparison between different periods of the experiment. The contours are in $\mu$s of relative arrival time.

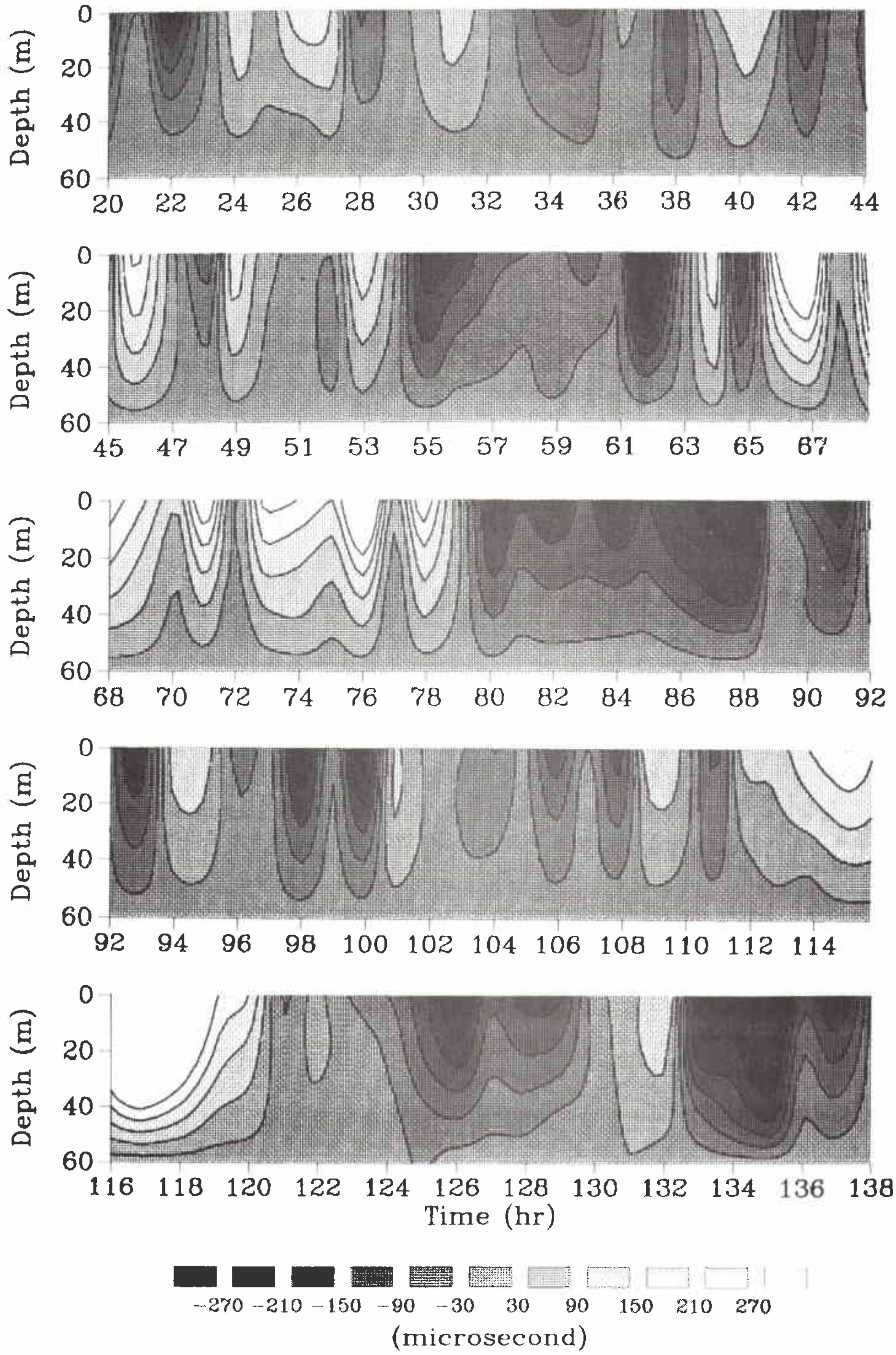


*Fig. 8b.* Corresponding contour plots for the refracted path. Note that the contour interval is three times greater than that used for the direct path.

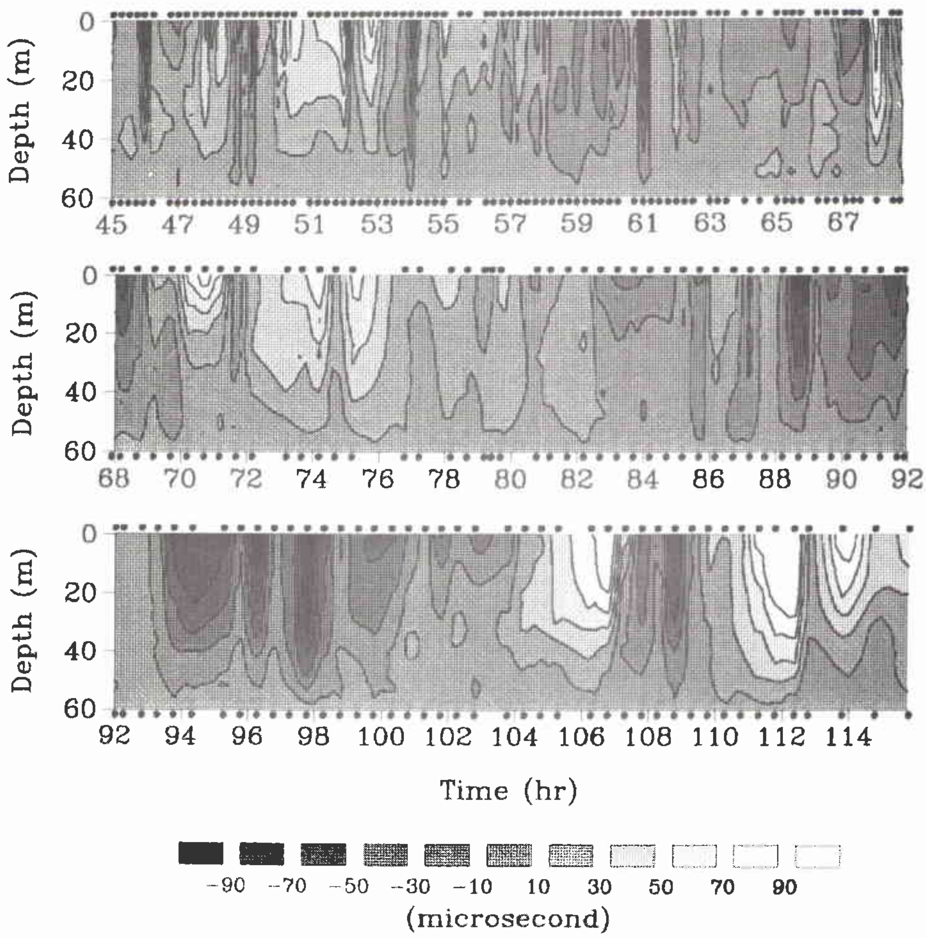


*Fig. 9a.* Contour plots of the direct-ray relative arrival time as for Fig. 8a but showing only those data taken at less than hourly intervals, not time-filtered. The event times are marked at the top and bottom of the contour sections by dots to show the sampling density. Some gaps occur where corrupted data have been removed.

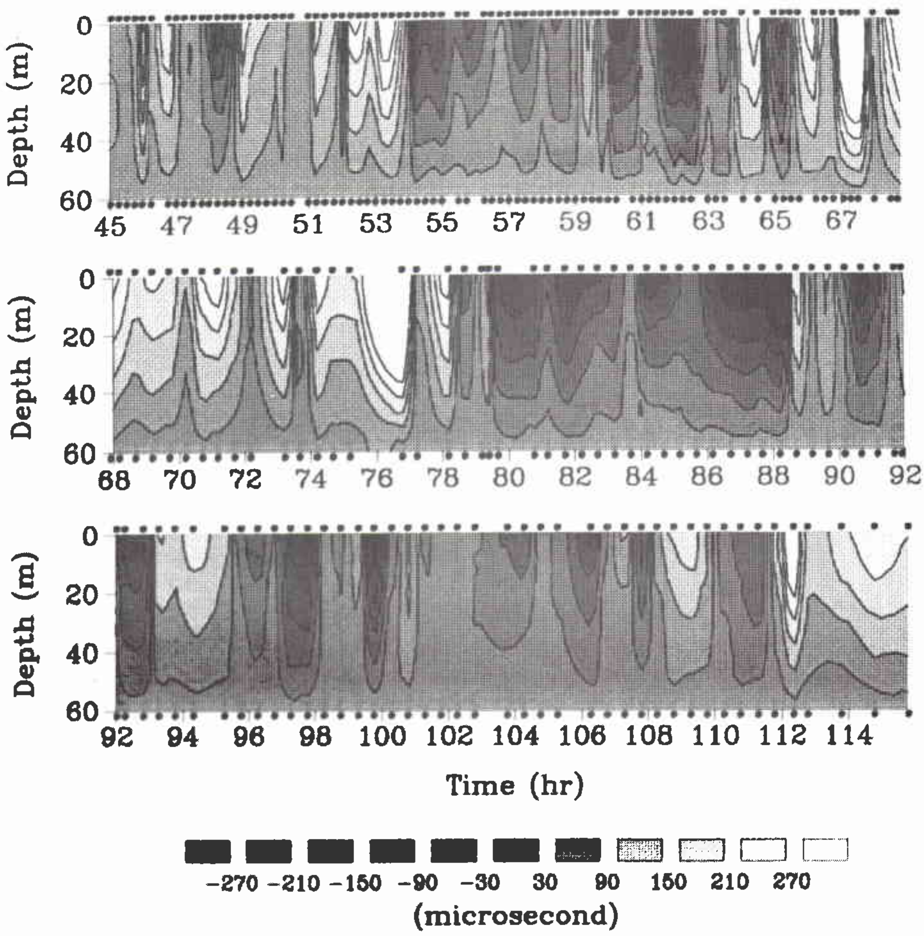


*Fig. 9b.* Contour plots for the refracted-ray relative arrival time as for Fig. 8b but unfiltered and with dots at the data points as in Fig. 9a.

# 4
# Environmental observations

## 4.1. APPLICABILITY OF INTERNAL-WAVE THEORY

The following TOB results have been obtained by a separate study [9], and will be quoted without proof. The TOB gives us a dense coverage of CTD data in both the horizontal and vertical directions. By incorporating navigational data from the towing ship and interpolating, a picture of the medium has been obtained in a vertical slice for each TOB run, most of which were of some 10 km length and spanned the depth range from 25 to 250 m. A two-dimensional dataset such as this is not usually available for acoustic experiments and allows us to describe the environment more fully. By examining the potential density field, it is possible to separate out the effects of internal waves from other features, which we shall call mixing intrusions.

Let $\alpha$ be the horizontal wavenumber of the refractive index variability. For high $\alpha$, in the region of $1.25 \times 10^{-2}$ m$^{-1}$, it has been found that internal waves may have contributed up to 25% of the sound-speed inhomogeneities. At lower $\alpha$, where there is much more activity, the internal-wave contribution becomes much less. An examination of the horizontal wavenumber spectra shows that they behave more like $\alpha^{-5/2}$, rather than like $\alpha^{-3/2}$, as would be expected from linear internal-wave theory. This analysis has made it clear that internal-wave activity makes a small, and possibly insignificant, contribution to the sound-speed inhomogeneity field down to 250-m depth. We have therefore been unable to use the familiar internal-wave theory to extrapolate our TOB measurements (taken over the depth range 25–250 m) to 400 m, the maximum depth encountered by the direct path ray. For intrusive mixing features which are approximately density-compensated with the background water, there are no well-behaved relationships to be found for the resulting sound-speed variations. It has therefore become necessary to look carefully at other environmental data, consisting of some 70 XBT drops and 8 CTD casts made from the MPG.

The TOB data provide full and accurate information as regards vertical and horizontal spatial, as well as temporal scales, but are lacking over a significant part of the depth range for the direct acoustic path. The CTD casts provide full and accurate data over all relevant depths but lack horizontal spatial information and are too few in number to give temporal information. The XBT casts give temperature data over the full depth range of interest and are of sufficient number to give temporal trends, but are inaccurate. By combining these three types of data it has been possible to build up a self-consistent model describing the sound-speed fluctuations imposed by the ocean.

### 4.2. EMPIRICAL MODEL OF THE SOUND-SPEED FLUCTUATIONS

The physical processes responsible for the fluctuations in the medium do not concern us here. We simply propose a three-layer model that describes the observed sound-speed fluctuations and which can be used in the appropriate acoustic propagation theory.

The structure function $D(x)$ of a function $f(y)$ is defined by

$$D(x) = \tfrac{1}{2}\langle [f(y) - f(y+x)]^2 \rangle. \tag{4}$$

If $f(y)$ is normalised to unit variance then in the limit as the ensemble average is taken over infinite data length, the structure function is related to the normalised autocorrelation function (acf) by

$$D(x) = 1 - \mathrm{acf}(x). \tag{5}$$

The vertical structure function of sound-speed fluctuations was calculated over various depth 'windows' within the TOB range. Since the statistics of the sound-speed inhomogeneities are non-stationary in the vertical an attempt was made to seek quasi-stationarity by taking subsets of the data over depth windows with a small depth range near the surface and larger depth ranges nearer the bottom. The depth range of each window was chosen to increase approximately exponentially with depth in an attempt to respect the natural vertical-scale size increase with depth in the ocean. A compromise was thus obtained between the requirement for quasi-stationarity and the limited length of data over which the structure function can be usefully calculated. The depth ranges of each of the 6 windows used are given in Table 1.

*Table 1*
Depth ranges

| | Window | | | | | |
|---|---|---|---|---|---|---|
| | 1 | 2 | 3 | 4 | 5 | 6 |
| Depth range (m) | 40–60 | 50–74 | 62–98 | 80–140 | 110–194 | 152–264 |
| Mean depth (m) | 50 | 62 | 80 | 110 | 152 | 208 |
| Depth span (m) | 20 | 24 | 36 | 60 | 84 | 114 |

A progressive increase in the characteristic length scale of the structure functions was found with increasing depth [9]. The vertical length scale increases over the range from the near-surface to about 100 m depth, but then remains roughly constant for greater depths, suggesting that the vertical scales of the intrusive mixing features are similar from 100 to 250 m. An examination of the CTD profiles shows that the salinity, temperature and sound speed are very highly correlated. A brief examination of the CTD and XBT casts indicates that the vertical scales from 250 to 400 m are about the same as for 100 to 250 m. In the absence of more complete data we shall consider the vertical structure function relevant to all depths between the source, at 400 m, and the uppermost receiver, at 224 m, to be equal to the structure function observed directly from the TOB data from 100 to 250 m.

The TOB data was also used to form the horizontal structure function of the sound-speed inhomogeneities at different depths down to 250 m. The depth dependence of these horizontal structure functions was found to be very weak. This is consistent with both an internal-wave field as well as with the mixing intrusions, discussed above, that are not density-controlled.

Let $\mu v'(x, y, z, t)$ be the randomly varying component of the sound speed, having zero mean and variance $\mu^2$. Consequently $v'$ has variance unity and we shall take the acf of $v'$ to be unity minus the structure function of $v'$. We shall denote the vertical, or dropped, acf of $v'$ by $V(\zeta)$, where

$$\zeta = z_1 - z_2. \tag{6}$$

Similarly, we shall denote the horizontal, or towed, acf of $v'$ by $H(\xi)$, where

$$\xi = x_1 - x_2. \tag{7}$$

Figure 10 shows both $V(\zeta)$ and $H(\xi)$ at a depth of $\sim$ 200 m. It can be seen from Fig. 10 that the measured vertical $V(\zeta)$ and horizontal $H(\xi)$ correlation functions of $v'$ are very similar in shape when the abscissae are suitably scaled. This close correspondence appears to hold over intervals relevant to the acoustic propagation i.e. separations of $\sim$ 60 m in the vertical, which is the length of the vertical array, and 5–6 km in the horizontal, the separation of source and vertical array. This means that a single empirical curve can be made to fit both $V(\zeta)$ and $H(\xi)$ in these intervals. A two-dimensional acf of $v'$ of the form $R(g)$ can be proposed, where

$$g^2 = (\zeta^2/L_\mathrm{v}^2 + \xi^2/L_\mathrm{h}^2). \tag{8}$$

Here $L_\mathrm{v}$ and $L_\mathrm{h}$ represent the vertical and horizontal scales of the irregular structures, and correspond to the scalings introduced in Fig. 10. The fact that $\zeta$ and $\xi$ appear as the sum of the squares implies an assumption of smoothness in the

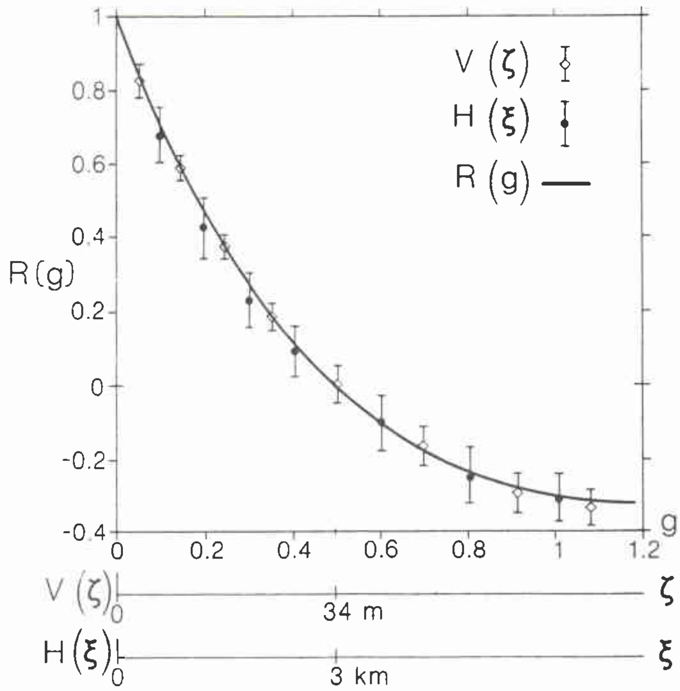


*Fig. 10.* Representative experimental values of $V(\zeta)$, denoted by diamonds, and those of $H(\xi)$, denoted by circles, both with their corresponding standard deviations. The best fit of the empirical model (9) is given by the full line. Note that the respective abscissae have different scales.

acf $R(g)$. It is easily recognised from the form of (8) that the inhomogeneities are modelled as ellipsoids.

An empirical curve with only two free parameters that gives a good fit to the measured values in Fig. 10 is

$$R(g) = \exp(-g)1 - g/l_2 + g^2/l_3^2. \tag{9}$$

This function is shown by the solid line in Fig. 10 for

$$l_2 = 0.45, \qquad l_3 = 1.60, \tag{10}$$

which values result from a best fit to the data in a least-mean-square sense. The corresponding values for $L_\mathrm{v}$, $L_\mathrm{h}$ are then

$$L_\mathrm{v} = 68 \text{ m}, \qquad L_\mathrm{h} = 6 \text{ km}. \tag{11}$$

The model of the sound-speed variations is completed by specifying how the inhomogeneity strength varies with depth. Although the form of the two-dimensional acf of the inhomogeneities $R(g)$ has been assumed to be depth-independent, the strength of the inhomogeneities will be approximated by a three-layer model.

Let $\eta^2$ be the variance of the refractive index. The values of $\mu^2$ and $\eta^2$ are linearly related (to first order for weak irregularities in the refractive index) with a factor of $v_0(z_0)^2$ between them, where $v_0(z_0)$ is a reference sound speed. Since the propagation theory is more conveniently represented in terms of $\eta^2$ we shall henceforth use $\eta^2$ instead of $\mu^2$. The value of $\eta^2$ as a function of depth is difficult to estimate. Examination of the XBT and CTD casts shows that the sound-speed variance about the mean profile does not decrease monotonically with depth. Rather, it exhibits a complex and variable depth dependence which includes a local maximum at ca. 300 m. This local maximum can be identified as due to detached intrusions of Levantine Intermediate Water (LIW) [8], which enters via the Sardinia–Sicily Channel, mixing with the background water type. The depth of these mixing intrusions is controlled by their density, and hence by the characteristic salinity and temperature of LIW. The depth range over which these intrusions affect the sound speed and the strength of the inhomogeneities produced are therefore constrained by the known properties of LIW. The sparcity of CTD casts and poor resolution of the XBT data do not justify any more than a simple three-layer model, for which approximate inhomogeneity strength estimates have been made.

The value of $\eta^2$ at 400 m is very low ($< 10^{-9}$), since internal waves are very unenergetic and the LIW mixing features are confined to shallower depths. We therefore choose $\eta^2 = 1 \times 10^{-9}$ for the bottom layer, 330 m $< z <$ 400 m. Over the depth range 270–330 m the LIW influence dominates, raising the value to between 1 and $2 \times 10^{-8}$ on average. We therefore choose $\eta^2 = 1.5 \times 10^{-8}$ for the middle layer, 270 m $< z <$ 330 m. From 220 to 270 m the value is well known (from the TOB data) and has a mean of $5 \times 10^{-9}$. We therefore choose $\eta^2 = 5 \times 10^{-9}$ for the upper layer, 220 m $< z <$ 270 m. It turns out that the final arrival-time structure is not very sensitive to the choice of values or layers for $\eta^2$, although the total phase fluctuation imposed is more directly affected.

# 5

# Propagation theory

## 5.1. THE RANDOM COMPONENT AND ITS CONNECTION WITH THE INHOMOGENEOUS REFRACTIVE INDEX

The direct rays are confined to depths between 224 and 400 m where the deterministic component of the sound-velocity profile is very nearly linear. In order to compare experimental results with theory we assume that the acoustic refractive index consists of a mean component $n_0(z)$ and a random component $\eta(z)n'(x,y,z,t)$ where $n'$ has zero mean and variance unity:

$$n(x,y,z,t) = n_0(z) + \eta(z)n'(x,y,z,t). \tag{12}$$

The mean velocity profile $v_0(z)$ and the mean refractive index are related by

$$n_0(z) = v_0(z_0)/v_0(z), \tag{13}$$

where $z_0$ is some reference depth, here taken to be $z_0 = 0$. The time for the pulse to travel from the origin to a hydrophone at depth $z$ on the vertical array by a ray path $z(x_1)$ terminating at this hydrophone can be calculated from the ray-path integral of the refractive index. Ignoring the effect of path curvature on path length, we obtain

$$\begin{aligned} T(X,z) &= v_0^{-1}(0)\left\{\int_0^X n_0[z(x_1)]\,\mathrm{d}x_1 + \int_0^X \eta[z(x_1)]n'[x_1,z(x_1)]\,\mathrm{d}x_1\right\} \\ &= T_0(X,z) + t(X,z), \end{aligned} \tag{14}$$

where

$$t(X,z) = v_0^{-1}(0)\int_0^X \eta[z(x_1)]n'[x_1,z(x_1)]\,\mathrm{d}x_1. \tag{15}$$

The effect of $\eta(z)n'(x_1,z)$ is to change the sound speed encountered along the path $z(x_1)$ (which directly affects the travel time) and also to perturb $z(x_1)$ about the deterministic path in the absence of inhomogeneities. In order to simplify the analysis we shall ignore the influence of $\eta(z)n'(x_1,z)$ on $z(x_1)$ as a lower-order contribution to the travel time and retain only the direct contribution to the sound speed encountered along the deterministic path. It is then clear from the properties of $n'$ that the ensemble average of $T$ gives the deterministic component, i.e.

$$\langle T(X,z)\rangle = T_0(X,z) = v_0^{-1}(0)\int_0^X n_0[z(x_1)]\,\mathrm{d}x_1. \tag{16}$$

It now follows from (1) and (3) that

$$\langle \tau(X,z) \rangle = T_0(X,z) - T_0(X,z'), \tag{17}$$

and that

$$r(X,z) = t(X,z) - t(X,z'). \tag{18}$$

The deterministic component $\langle \tau(X,z) \rangle$ and the stochastic residuals $r(X,z)$ can now be compared with theory since they have been related to properties of the acoustic refractive index within the body of the medium.

### 5.2. STRUCTURE FUNCTION OF THE TIME DELAYS

Comparison of the random component of the arrival-time delay with theoretical predictions is best made by considering the structure function of $r$, which we shall denote by $D_r(\zeta)$. Clearly, from (18) the structure function of $r(X,z)$ is the same as that of $t(X,z)$, both of which will henceforth be denoted by $D(\zeta)$. From (15) we obtain

$$D(\zeta) = \int_0^X \int_0^X [\eta/v_0(0)]^2 \{R[x_1 - x_2, 0] - R[x_1 - x_2, z_1(x1) - z_2(x_2)]\} \, \mathrm{d}x_1 \, \mathrm{d}x_2, \tag{19}$$

where

$$R[x_1 - x_2, z_1(x_1) - z_2(x_2)] = R(\xi, \zeta) = \langle n'(x_1, z_1) n'(x_2, z_2) \rangle. \tag{20}$$

The acf of random refractive-index variations is (to first order for weak irregularities) the same as that of the sound-speed variations (9), apart from a constant factor. In addition, the mean component of the refractive index $n_0(z)$ is almost a linear function of $z$ between 224 and 400 m so that the deterministic ray paths are given by the arcs of circles:

$$z_1(x_1) = z_1(X) x_1^2/X^2, \qquad z_2(x_2) = z_2(X) x_2^2/X^2. \tag{21}$$

Let

$$\zeta(X) = z_1(X) - z_2(X), \qquad Z = \tfrac{1}{2}[z_1(X) + z_2(X)], \tag{22}$$

so that

$$D[\zeta(X)] = v_0(0)^{-2} P[0] - P[\zeta(X)], \tag{23}$$

where

$$P[\zeta(X)] = \sum_{i=0}^{2} \eta_i^2 \int_{a_i}^{a_{i+1}} \int_{a_i}^{a_{i+1}} \exp(-g)(1 - g/l_2 + g^2/l_3^2) \, \mathrm{d}x_1 \, \mathrm{d}x_2, \tag{24}$$

obtained by substitution into (9), and where

$$g = \left\{[(Z + \zeta(X)/2)x_1^2 - (Z - \zeta(X)/2)x_2^2]^2/(X^4 L_v^2) + (x_1 - x_2)^2/L_h^2\right\}^{1/2}, \quad (25)$$

obtained by substitution into (8). The $a_i$ are the values of $x$ at which the path integral intersects the interfaces between the three layers of the inhomogeneity model. The integral has therefore been split into a sum of three parts, each with a different, but constant, value of $\eta^2$. The expression (23) for $D(\zeta)$ was evaluated for the following values of the parameters and constants:

$$Z = 144 \text{ m}, \qquad X = 5000 \text{ m}, \qquad L_v = 68 \text{ m}, \qquad L_h = 6000 \text{ m},$$

$$v_0(0)^2 = 2.25 \times 10^6 \text{ m}^2\text{s}^{-2},$$

$$a_0 = 0, \qquad a_1 = 0.82, \qquad a^2 = 0.92, \qquad a_3 = 1,$$

$$\eta_1^2 = 5 \times 10^{-9}, \qquad \eta_2^2 = 1.5 \times 10^{-8}, \qquad \eta_3^2 = 1 \times 10^{-9}.$$

The result is shown in Fig. 11 together with the structure function evaluated directly from the observed time delays. The agreement between experiment and theory is seen to be within observational error at all evaluated points. The consistently higher values of the theoretical structure function may be due to over-estimation of $\eta^2$ in one or more of the layers. The structure function continues to rise strongly up to the maximum lag (62 m) observed, confirming that the characteristic vertical spatial length is larger than the vertical array length.

### 5.3. *THE QUANTITIES* $\Gamma$ *AND* $\chi$

In order to place NAPOLI '85 in context with other scattering experiments, we shall evaluate two important parameters, denoted $\Gamma$ and $\chi$, which serve to characterise the scattering regime. $\Gamma$ is a measure of the scattering strength of the medium; high values ($> 1$) indicate that multiple scattering will occur within one Fresnel length. $\chi$ is the range of propagation, scaled by the Fresnel length; high values ($> 1$) indicating that phase modulations imposed by the scattering will be fully developed into amplitude fluctuations. Moreover, the product $\Gamma\chi$ is simply the variance of the phase fluctuation $\langle\phi^2\rangle$ imposed by the random part of the medium along the path from source to receiver. A knowledge of $\Gamma$ and $\chi$ enables us to locate NAPOLI '85 in the $\Gamma$, $\chi$ plane (see, for example, Ewart et al. [10]), which determines whether the propagation is subject to sparse (single) or frequent (multiple) scattering and the degree of development of the resulting phase modulations. We are now in a position to make estimates of these quantities, defined as

$$\Gamma = k^3\langle\eta^2\rangle L_H L_V^2, \qquad \chi = X/(kL_V^2), \quad (26)$$

where $k$ is the acoustic wavenumber and $L_H$ and $L_V$ are horizontal and vertical scale sizes of the sound-speed inhomogeneities (see, for example, Ewart et al. [10]). We

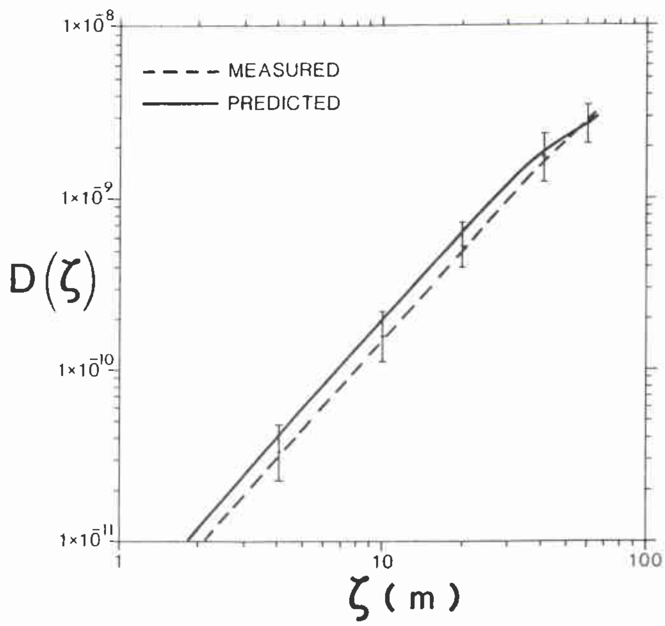


*Fig. 11.* Structure function formed from the stochastic component of the arrival times for all 229 events shown together with the best fit theoretical curve and standard error limits.

are not able to apply the normal definition of $L_{\mathrm{H}}$ or $L_{\mathrm{V}}$ to our finite data, since the definition involves an integral of the acf over infinite limits. $L_{\mathrm{h}}$ and $L_{\mathrm{v}}$ are also intended to be representative lengths, single values which serve to characterise an acf whose form is roughly known. There is no exact relationship between $L_{\mathrm{H}}$ and $L_{\mathrm{h}}$ or $L_{\mathrm{V}}$ and $L_{\mathrm{v}}$ for a general acf, but the values are not likely to differ by more than a factor of 2. For the purposes of characterising the scattering regime, we shall substitute $L_{\mathrm{h}}$ for $L_{\mathrm{H}}$ and $L_{\mathrm{v}}$ for $L_{\mathrm{V}}$. Also, the ensemble average $\langle\eta\rangle^2$ over the whole ray-path becomes an integral, since our $\eta$ is a function of depth. The resulting values of $\Gamma$ and $\chi$ are given in Table 2, with the value for $\langle\phi^2\rangle$, for the acoustic frequencies 250 and 2 kHz.

It can be seen from the values of $\Gamma$, $\chi$ that NAPOLI '85 spans a region from very weak to mild multiple scattering. This is a useful range for the purposes of investigating the ocean transfer function since the modulations of the acoustic signal imposed by the ocean will be fairly smooth and progressive from lower to higher frequencies.

*Table 2*
Resulting values

| | Acoustic frequency (Hz) | |
|---|---|---|
| | 250 | 2000 |
| $\Gamma$ | 0.16 | 82 |
| $\chi$ | 1.08 | 0.14 |
| $\langle\phi^2\rangle$ | 0.17 | 11.5 |

### 5.4. A SIMPLE APPROACH

The four components of observed acoustic fluctuations, environmental measurements, empirical ocean inhomogeneity model and scattering theory have been linked together in the above sections and shown to be in mutual agreement. In the theoretical section the scattering theory was developed to accept the empirical model for the sound-speed inhomogeneities as input. If an acf of the sound-speed inhomogeneity field is input to the scattering theory, the acf of the arrival-time fluctuations will be output, which yields not only the total phase modulation, but also the temporal and spatial structure of the fluctuations. A simpler approach would be to use only characteristic lengths of the sound-speed inhomogeneities, instead of the full acf. The scattering theory would then be simpler, and would only yield the total phase fluctuation, rather than the vertical spatial structure.

Suppose we develop a very simple model, using the same basic assumptions and approximations, as follows. Let the direct path have a length equal to the range $X$. Taking (12) and (13) it is easy to show that the velocity $v$ is given by

$$v(x,y,z,t) = v_0(z) - \eta n'(x,y,z,t)\, v_0(z). \tag{27}$$

Let the horizontal correlation distance of the ocean inhomogeneities be $L_{\mathrm{h}}$ and the vertical correlation length be $L_{\mathrm{v}}$ as before. Assume, as before, that the direct ray path is not altered by the inhomogeneities but that only the travel time is affected by the different sound-speed patches encountered along the path. Let us further assume that the direct-ray path has a mean inclination $\theta$ to the horizontal, where

$$\mathrm{mod}\,|\tan\theta| \ll L_{\mathrm{v}}/L_{\mathrm{h}}, \tag{28}$$

so that the projected correlation length of the inhomogeneities along the path is approximately $L_{\mathrm{h}}$. The ray-tracing results show that the direct path satisfies this criterion, except near the end of the path, where $\tan\theta \simeq 0.02$, whereas $L_{\mathrm{v}}/L_{\mathrm{h}} = 0.01$.

The condition (28) is therefore not strictly satisfied over the whole path. The $j$th inhomogeneity will impose a travel-time delay on the $i$th event, $\tau_{ij}$, of approximately

$$\tau_{ij} = L_{\mathrm{h}}\eta / v_0(z_0). \tag{29}$$

The scattering encountered will be uncorrelated from one scattering inhomogeneity to the next and the time deviations will then add up as a sum of squares to give the total ensemble average time delay

$$\langle t^2 \rangle = X/L_{\mathrm{h}} \langle [L_{\mathrm{h}}\eta / v_0(z_0)]^2 \rangle. \tag{30}$$

The variance in the random arrival time delays $\langle t^2 \rangle$, for the 5-km path can be obtained from $\langle \phi^2 \rangle$ by

$$\langle t^2 \rangle = \langle \phi^2 \rangle / [k v_0(z_0)]^2, \tag{31}$$

which yields

$$\langle \phi^2 \rangle = X L_{\mathrm{h}} k^2 \langle \eta^2 \rangle. \tag{32}$$

This is exactly the expression obtained for $\langle \phi^2 \rangle$ obtained by evaluating the product $\Gamma\chi$ from (26) above. The result for the total phase modulation can therefore be more easily obtained by a much simpler approach. The simple approach above does not, however, provide us with the time or vertical spatial correlation.

# 6

# Summary

NAPOLI '85 was an acoustic experiment designed to measure the variability in the ocean transfer function down a vertical array and with time over a path length of 5 km in the frequency range 250 Hz to 2 kHz. The stability of the weather and array systems allowed an additional analysis to be made, that of vertical spatial and temporal relative arrival-time fluctuations. The results have been presented in this memorandum. Two major ray-paths connected source and receivers, a surface-refracted and a lower-refracted (direct) path. Analysis of the relative delay times for the direct path observed in NAPOLI '85 revealed a deterministic component which was very close to that expected from ray theory and which remained stable throughout the five days of the experiment. In addition to the deterministic component, there was a superimposed stochastic component. The strength of the stochastic component was some three times greater for the surface refracted ray, compared to the direct ray, although spatial and temporal scales are similar. Typical rms values are 60 $\mu$s for the direct path and 180 $\mu$s for the upper-refracted path.

Analysis [9] of the environmental data has shown that internal-wave theory is not applicable to the sound-speed inhomogeneities encountered in the medium. Several types of environmental data have been combined with an understanding of the physical oceanography to develop an empirical model for the spatial autocorrelation function of sound-speed inhomogeneities for NAPOLI '85. A vertical scale $L_{\mathrm{v}}$ and a horizontal scale $L_{\mathrm{h}}$ result from this model. These data have also been used to evaluate a simple three-layer model of the variance of the refractive index $\eta^2$ which describes both the strength and spatial structure of the ocean variability.

A theoretical structure function for relative arrival times down the vertical array for the direct path was derived using our empirical spatial autocorrelation function. This theoretical curve was compared with the experimental structure function of the random relative arrival times and good agreement was found. Thus the random component of the relative delay times can be accounted for satisfactorily.

# References


[1] Ewart, T.E. Acoustic fluctuations in the open ocean – A measurement using a fixed refracted path. *Journal of the Acoustical Society of America*, **60**, 1976: 46–59.

[2] Ewart, T.E. and Reynolds, S.A. The mid-ocean acoustic transmission experiment (MATE). *Journal of the Acoustical Society of America*, **75**, 1984: 785–802.

[3] Ellinthorpe, A.W. The Azores range. Tech. Doc. 4551. New London CT, Naval Underwater Systems Center, April 1973.

[4] Uscinski, B.J. and Macaskill, C. Frequency cross-correlation of intensity fluctuations in multiple scattering. *Optica Acta*, **32**, 1985: 71–89.

[5] Miller, S.J. and Uscinski, B.J. Frequency cross-correlation of intensity fluctuations. Limitations of multiple scatter solutions. *Optica Acta*, **33**, 1986: 1341–1358.

[6] Ewart, T.E., Macaskill, C. and Uscinski, B.J. The MATE acoustic frequency cross-correlation of intensity. *Journal of the Acoustical Society of America*, **77**, 1985: 1732–1741.

[7] Molcard, R. and Tait, R.I. The steady state of the step structure in the Tyrrhenian Sea. *ed.* Angel, M. A Voyage of Discovery. Oxford, Pergamon, 1977: 221–233.

[8] Hopkins, T.S. and Zanasca, P. Oceanographic data from the southern Tyrrhenian Sea: August–October 1984, Part 1: Floats and moored instruments, Part 2: Hydrography. SACLANTCEN SM-198. La Spezia, Italy, SACLANT Undersea Research Centre, 1988.

[9] Potter, J.R. Oceanographic fluctuations during NAPOLI '85, an experiment in the Tyrrhenian Sea. (SACLANTCEN document, in preparation.)

[10] Ewart, T.E., Macaskill, C. and Uscinski, B.J. Intensity fluctuations, Part II: Comparison with the Cobb Experiment. *Journal of the Acoustical Society of America*, **74**, 1983: 1484–1499.

Report no. changed (Mar 2006): SM-223-UU

## Initial Distribution for SM-223

| | |
|---|---|
| *Ministries of Defence* | |
| JSPHQ Belgium | 2 |
| DND Canada | 10 |
| CHOD Denmark | 8 |
| MOD France | 8 |
| MOD Germany | 15 |
| MOD Greece | 11 |
| MOD Italy | 10 |
| MOD Netherlands | 12 |
| CHOD Norway | 10 |
| MOD Portugal | 5 |
| MOD Spain | 2 |
| MOD Turkey | 5 |
| MOD UK | 20 |
| SECDEF US | 60 |
| *NATO Authorities* | |
| Defence Planning Committee | 3 |
| NAMILCOM | 2 |
| SACLANT | 3 |
| SACLANTREPEUR | 1 |
| CINCWESTLANT/ COMOCEANLANT | 1 |
| COMSTRIKFLTANT | 1 |
| CINCIBERLANT | 1 |
| CINCEASTLANT | 1 |
| COMSUBACLANT | 1 |
| COMMAIREASTLANT | 1 |
| SACEUR | 2 |
| CINCNORTH | 1 |
| CINCSOUTH | 1 |
| COMNAVSOUTH | 1 |
| COMSTRIKFORSOUTH | 1 |
| COMEDCENT | 1 |
| COMMARAIRMED | 1 |
| CINCHAN | 3 |
| *SCNR for SACLANTCEN* | |
| SCNR Belgium | 1 |
| SCNR Canada | 1 |
| SCNR Denmark | 1 |
| SCNR Germany | 1 |
| SCNR Greece | 1 |
| SCNR Italy | 1 |
| SCNR Netherlands | 1 |
| SCNR Norway | 1 |
| SCNR Portugal | 1 |
| SCNR Turkey | 1 |
| SCNR UK | 1 |
| SCNR US | 2 |
| SECGEN Rep. SCNR | 1 |
| NAMILCOM Rep. SCNR | 1 |
| *National Liaison Officers* | |
| NLO Canada | 1 |
| NLO Denmark | 1 |
| NLO Germany | 1 |
| NLO Italy | 1 |
| NLO UK | 1 |
| NLO US | 1 |
| *NLR to SACLANT* | |
| NLR Belgium | 1 |
| NLR Canada | 1 |
| NLR Denmark | 1 |
| NLR Germany | 1 |
| NLR Greece | 1 |
| NLR Italy | 1 |
| NLR Netherlands | 1 |
| NLR Norway | 1 |
| NLR Portugal | 1 |
| NLR Turkey | 1 |
| NLR UK | 1 |

| | |
|---|---|
| Total external distribution | 236 |
| SACLANTCEN Library | 10 |
| Stock | 34 |
| Total number of copies | 280 |